# Experiments to Systematically Evaluate the Role of Cohesion in River Morphodynamics

Nacere Mohamed Samassi[1,2], Fernando David Cúñez[1], and Rachel C. Glade[1,2]

[1]University of Rochester, Department of Earth and Environmental Sciences, 120 Trustee Rd, Rochester, NY, 14620.

[2]University of Rochester, Department of Mechanical Engineering, 235 Hopeman Building, P.O. Box 270132, Rochester, NY, 14627-0132

[1]To whom correspondence should be addressed. Email: nsamassi@ur.rochester.edu

**This manuscript is a non-peer reviewed preprint that has been submitted to EarthArXiv. The paper has been submitted to Geology for peer review. Updated versions will be uploaded as the paper (hopefully) traverses the peer review process.**

**ABSTRACT**

While cohesion is thought to be an important control on sediment transport, few studies have systematically examined the role of cohesion in river morphodynamics. In this study we use simplified, small-scale laboratory experiments to investigate how increasing sediment cohesion affects the morphometrics of fluvial channels. Experiments were conducted in a laminar flume with a mixture of angular, sand-sized plastic particles and different amounts of xanthan gum—a proxy for cohesive biofilms—to tune cohesion among grains. With increasing cohesion, we observe a transition from highly mobile, braided to single thread meandering channels, then to straight, gully-like channels with headcuts that exhibit decreasing distance of retreat with increasing cohesion. Particle image velocimetry (PIV) shows that cohesion decreases sediment transport rate even when discharge is increased, suggesting an increase in critical shear stress. Bank width measurements show that this leads to narrowing of the channel with increasing cohesion. However, strong qualitative differences in observed channel morphodynamics suggest that beyond changing critical shear stress, cohesion alters the fundamental processes that govern channel erosion, including bank strength and the formation of aggregates. Our work suggests a novel approach of using sediment cohesion to explore the transition between transport limited and detachment limited channels.

## 1. INTRODUCTION

Natural alluvial rivers exhibit a variety of forms including braided rivers (Figure 1A), single thread meandering rivers (Figure 1B), and gully-like channels with steep, retreating headcuts (Figure 1C). Previous work suggests that cohesion may be an important factor determining different river forms. Laboratory experiments have illustrated that bank cohesion is needed to transition from braided to single-thread channels (Parker 1976; Van Dijk et al., 2013; Tal & Paola, 2010; Brauderick et al., 2009; Peakall et al., 2007). While vegetation is a primary source of bank cohesion on Earth (Brauderick et al., 2009), other sources include abundant fine sediment, permafrost, and chemical cementation that may explain paleo single thread meandering channels found on Mars (Lapotre et al., 2019; Matsubara et al., 2015). Further, cohesion may control channel width as it increases the critical shear stress of the banks (Kothyari and Jain, 2008; Rahimnejad and Ooi, 2016; Zhang and Yu, 2017; Dunne and Jerolmack 2020; Brunier-Coulin et al., 2020; Sharma et al., 2022; Chen et al., 2022) (Figure 1D, E), resulting in narrower threshold channels in both gravel bed rivers (e.g., Andrews 1984; Huang and Warner 1995) and sand bed rivers (Kleinhans et al., 2015; Dunne and Jerolmack 2018, 2020). In a different fluvial setting, cohesion may also influence the formation of gullies, rapidly eroding new channels that often form in response to disturbance (Bennett and Wells, 2019). Tucker et al., 2006 propose that in order to form gullies, cohesion must be low enough to allow rapid erosion of sediment (e.g., de-vegetated agricultural lands (Prosser and Slade, 1994)), yet high enough to maintain steep banks and a retreating headcut characteristic of gullies (Kirby and Bracken 2009). Cohesive soil is also needed to produce experimental gullies in the lab (e.g., Day et al., 2018; Bennett et al., 2000). While previous work suggests the importance of cohesion in fluvial erosion in different settings, cohesion controls on river morphodynamics have never been systematically evaluated. Here we present the results of a series of simplified experiments in a laminar flume to determine how systematically increasing cohesion affects channel evolution, thus enhancing our understanding of geomorphic systems in both natural and human altered landscapes.

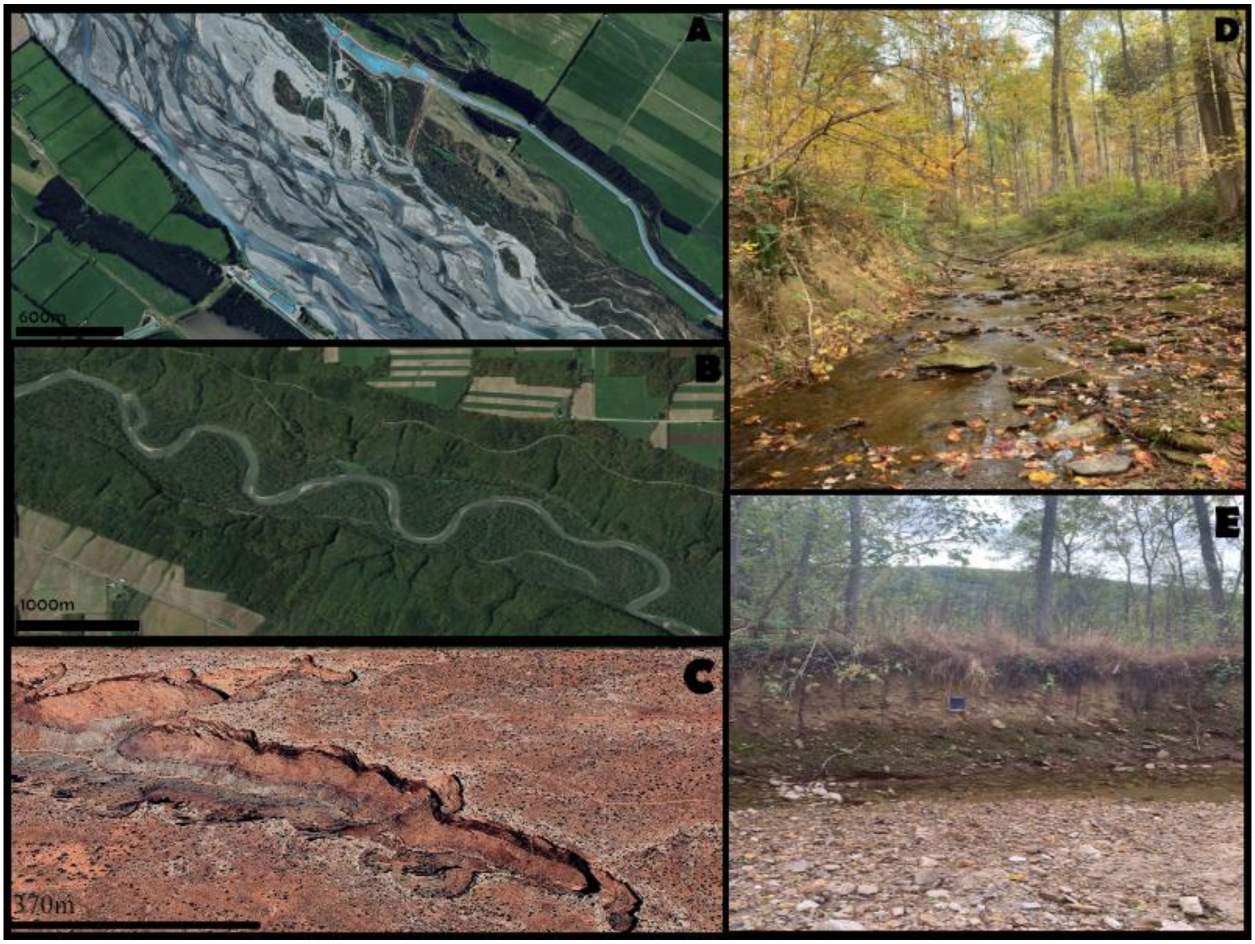


Figure 1

## 2. METHODS

We conducted laboratory experiments in a laminar flume (Figure 2A) to explore how systematically increasing levels of cohesion alter channel dynamics, focusing on planform channel shape and headcut propagation. Inspired by a recent study that explored the role of cohesion in fluvial ripple experiments (Malarkey et al., 2015), we use xanthan gum to tune cohesion. Xanthan gum, a polysaccharide secreted by the bacterium Xanthomonas campestris (Rosalam and England, 2006), is an appealing source of cohesion because 1) it is a type of extracellular polymeric substrate (EPS) produced by microbes that can be found in many natural landscapes (Jones et al., 2024) and has been used by humans to stabilize river banks (Smith et al., 2022) and soils (Chen C., et al., 2019), 2) is very inexpensive, 3) is easy to mix with sediment, and 4) when wetted and subsequently dried, xanthan gum forms bridges between grains (Figure 2C) that maintain cohesive properties for a sufficient duration in our experiments (~1 hour) even when fully submerged. We used angular, sand sized plastic particles (MultiBlast Type II) with a density of 1190 kg/m^3 and particle diameters ranging from 0.25 to 0.42 mm that allowed us to maintain clear water and laminar flow conditions (SI1).

Experiments were conducted in a 1m long, 20cm wide laminar flume at a slope of ~.002 with recirculating water, but no sediment recirculation. The base level condition was a 1 cm tall, 2 cm wide notch in the center of the flume outlet wall which promoted channelization and headcut retreat (Figure S1). A small notch at the inlet wall and a gently scraped initial straight depression allowed the channel to form in the middle of the flume. We prepared mixtures of 2300g of plastic particles with varying concentrations of xanthan gum (%XG) from 0 to 0.5% by weight (beyond 0.5% XG, sediment transport was no longer possible in our flume setup at maximum discharge). These percentages are in line with preliminary measurements of EPS concentrations found in natural soils (Jones et al., 2024). 1000 ml of water was added to each mixture, which was then evenly distributed across the flume bed at a depth of 2 cm. To ensure consistent compaction between experiments, we compressed the bed mixture using a 105 cm long, 17.2cm thick wooden log, applied for 20 minutes. We allowed a drying period of about 24 hours before initiating the experiments to activate the xanthan gum bonds that produce cohesion between grains (Figure 2C). For each experiment, we began with a low flow rate to fill the initial shallow channel, then slowly increased the flow rate until we observed the beginning of sediment transport. Discharges needed to move sediment were 25 L/hour for 0-0.2% XG, 40

L/hour for 0.3%XG, and 55 L/hour for 0.4-0.5%XG. Experiments were run until the channel either migrated to the sidewalls (low %XG runs) or stopped evolving entirely (high %XG runs) for a range of 20-140 minutes. We analyzed top-down experimental videos captured at 60fps to obtain sediment velocities using PIVlab, and channel width and headcut retreat rate using ImageJ (SI1). A second set of experiments showed that qualitative channel morphology changes due to cohesion are reproducible (SI2).

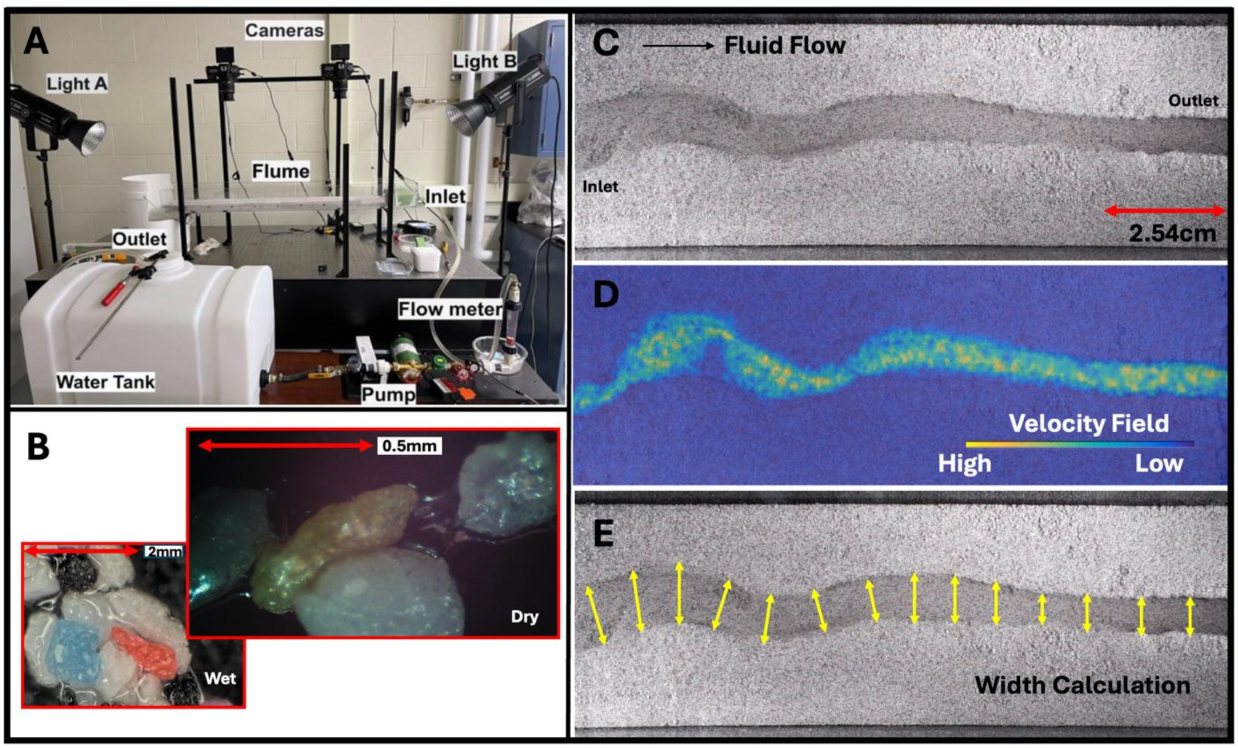


Figure 2

## 3. RESULTS AND INTERPRETATION

Qualitatively, our experiments show that with increasing cohesion (and co-varying increasing discharge), channels transition from a wide, highly mobile braided stream (0%XG) to a more single thread meandering stream (0.1%XG), to a narrower single thread straight channel with a rapidly retreating headcut, (0.2%XG), and finally to short, narrow dendritic channels with headcuts that retreat more slowly as %XG increases (0.3-0.5%XG) (Figure 3). As %XG increases, bank erosion transitions from single grain removal to discrete bank collapse events that produce aggregates (0.2% and higher). See Supplemental Videos.

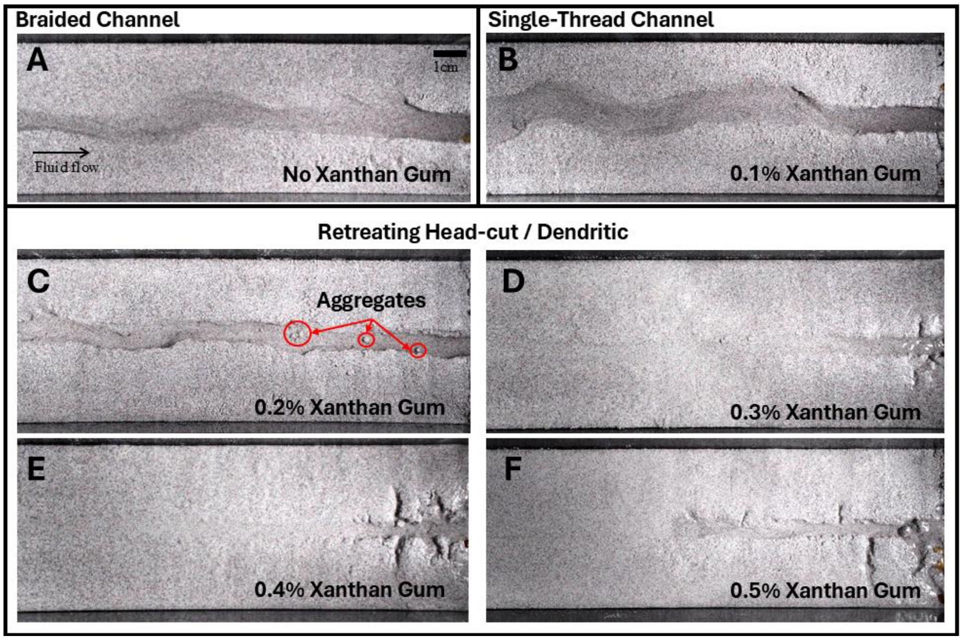


Figure 3:

ImageJ analysis shows that bank widths (Figure 4A) generally decrease with increasing cohesion, indicating that higher %XG results in a narrower lateral movement over time, even with higher discharge. Standard deviations show that channel widths exhibit more variability for low %XG, while the higher percentages xanthan gum exhibit more narrow and stable channels (Figure 4A). There is a clear change in behavior between 0.1 and 0.2%XG in which the channel narrows to approximately 2cm, the width of the outlet notch. We are confident that this is due to increasing cohesion alone, as discharge remained constant for 0-0.2%XG. Additionally, at 0.2%XG and higher we observe the onset of well-defined retreating headcuts.

To explore bank widening and headcut retreat trends, we fit our data with an assumed equation of the form $w(t), h(t) = w_f, h_f(1 - e^{-\frac{t}{t_s}})$ (Eqn.1), where *w(t)* and *h(t)* represent the width and head cut position of the channel at time *t*, $t_s$ is a characteristic timescale of adjustment, and $w_f$ and $h_f$ are the final values once the channel stops evolving (Figure 4A,B). Although experiments at lower %XG could not be run long enough to achieve complete steady state, fitted $w_f$ values clearly show the narrowing of expected steady state widths as %XG increases. Widths are slightly higher for 0.4-0.5%XG due to bank collapse at the outlet, likely enhanced by the higher discharge required for those experiments. Observations of headcut location through time show that at 0.2%XG, the channel exhibits a near constant headcut retreat rate of ~1.2cm/min and keeps retreating until it reaches the inlet. For higher %XG runs, while initial retreat rate is similar, final headcut retreat distance decreases with increasing cohesion. These data support the interpretation that cohesion strongly suppresses the rate and extent of bank widening and head-cut migration. Further, the development of retreating headcuts at higher %XG indicates that XG may allow continuous exploration of channel morphodynamics on a spectrum ranging from transport limited to detachment limited channels (Vachtman and Laronne, 2013).

PIV analysis shows that average sediment velocities tend to decrease with increasing %XG, despite an increase in discharge (Figure 4C). Empirical sediment transport relationships (e.g., Meyer-Peter Müller 1948; Parker 1990) show that the mean grain velocity $U_{mean}$ scales with shear stress $\tau$ above a critical threshold $\tau_c$, typically following a power-law form: $U_{mean} \propto (\tau - \tau_c)^{3/2}$. In our experiments, while discharge (and therefore $\tau$) increases across runs, we observe a decrease in mean grain velocity as xanthan gum concentration rises. This indicates that cohesion substantially raises the critical shear stress, suppressing grain motion under stronger flows. While previous work has determined a modified shields stress equation for cohesive sediment under an impinging jet (Brunier-Coulin et al., 2020; Sharma et al., 2022), further experiments are needed to quantify the critical shear stress in the presence of cohesion for shear flows. Our PIV results generally support the idea that channel narrowing and slowing of headcut retreat with increasing %XG is largely due to an increase in the critical shear stress, as expected for threshold channels (Parker 1978; Phillips and Jerolmack 2016; Phillips et al., 2022). However, it is interesting that average sediment velocities are constant for 0-0.2%XG (Figure 4C left side), despite different time and space averaged channel widths for each case (Figure 4C right side). This suggests that cohesion controls on channel morphology beyond simple changes in critical shear stress, likely due to differences in channel erosion mechanisms with increased bank strength (Delenne et al., 2004) and the formation of aggregates that can alter the flow path by reducing the effective cross-sectional area available for water movement (Perret et al., 1999).

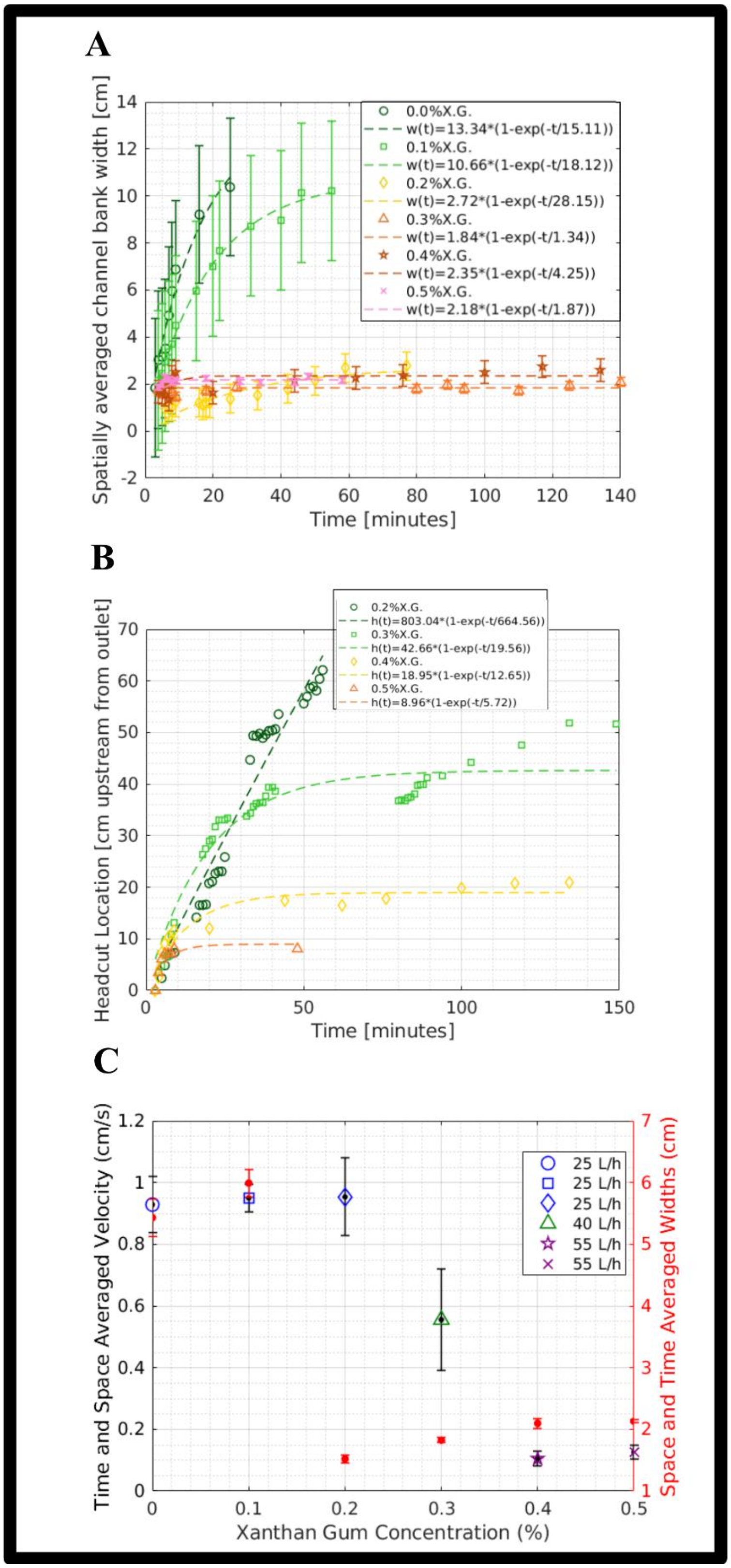
A
Spatially averaged channel bank width [cm]
Time [minutes]
0.0%X.G.
w(t)=13.34*(1-exp(-t/15.11))
0.1%X.G.
w(t)=10.66*(1-exp(-t/18.12))
0.2%X.G.
w(t)=2.72*(1-exp(-t/28.15))
0.3%X.G.
w(t)=1.84*(1-exp(-t/1.34))
0.4%X.G.
w(t)=2.35*(1-exp(-t/4.25))
0.5%X.G.
w(t)=2.18*(1-exp(-t/1.87))
B
Headcut Location [cm upstream from outlet]
Time [minutes]
0.2%X.G.
h(t)=803.04*(1-exp(-t/664.56))
0.3%X.G.
h(t)=42.66*(1-exp(-t/19.56))
0.4%X.G.
h(t)=18.95*(1-exp(-t/12.65))
0.5%X.G.
h(t)=8.96*(1-exp(-t/5.72))
C
Time and Space Averaged Velocity (cm/s)
Space and Time Averaged Widths (cm)
Xanthan Gum Concentration (%)
25 L/h
25 L/h
25 L/h
40 L/h
55 L/h
55 L/h

Figure 4:

## 4. DISCUSSION AND CONCLUSIONS

Our results provide experimental evidence that cohesion can fundamentally alter channel morphodynamics. As suggested in previous studies with vegetation (e.g., Brauderick et al., 2009), cohesion is needed to produce a single thread channel. Observations of channel narrowing with increasing %XG along with PIV analysis of grain velocities suggest that cohesion controls channel morphology both by altering the critical shear stress (e.g., Dunne and Jerolmack 2020) and allowing for qualitative differences in bank erosion processes, such as bank collapse and the formation of aggregates. Moving beyond previous experiments, we show that further increasing cohesion leads to gully-like channels with retreating headcuts. Increasing xanthan gum concentration reduces both the rate and extent of channel adjustment. Low-cohesion cases widen gradually over more extended periods, while higher cohesion leads to quicker transitions toward equilibrium with smaller final widths and retreat distances. The 0.2% xanthan gum case with a constantly retreating headcut supports the idea of a goldilocks case in which cohesion is strong enough to hold the bank of the headcut but too weak to stop ongoing bed erosion and retreat, as seen in persistent gullies (Tucker et al., 2006). Further experiments would be needed to explore how ephemeral flows characteristic of gullies affect cohesive channel morphology. Overall, we propose that Xanthan gum is an ideal way to systematically control cohesion in flume experiments, allowing continuous exploration of channel morphodynamics on a spectrum ranging from transport limited to detachment limited channels.

At higher cohesion levels (0.3-0.5), we observe the formation of side channels**,** a departure from the single-thread morphologies typically expected in stable cohesive systems (Tal & Paola, 2007). First, this behavior suggests that discrete, cohesive bank failure events may allow secondary pathways to emerge during high flow conditions (Julian & Torres, 2006). Side channels may also develop due to variations in cohesion throughout the substrate mixture, where areas of lower cohesion create weak points that allow fluid shear forces to dislodge the grains. Another possible mechanism for the formation of side channels is the fact that the higher discharge needed to transport cohesive sediment encourages overland flow, allowing water to find more possible paths to follow. While at first glance this may just be an artefact of our experimental setup, it is possible that a similar two-part effect occurs in nature. First, in highly cohesive sediment, deeper overland flow (and therefore larger storms) may be needed to surpass the threshold of motion for sediment and initiate channels. Second, slow channel development and headcut retreat may allow abundant water to find alternate flow paths at steep, newly formed channel banks, producing secondary channels. Factors such as soil type and climate can influence both cohesion and drainage density, ultimately affecting erosion processes (Moeini, et al., 2015; Moragoda et al., 2022).

Our simplified experiments have a number of limitations. While our experiments were conducted in laminar/transitional flow, sediment entrainment in natural rivers is primarily governed by turbulence (Wilcock et al., 2003). The presence of turbulence may dampen cohesive effects by more efficiently dislodging aggregates. Our experiments also were not able to record water or channel depth, which would be needed to accurately estimate shear stress and 3D channel geometry. Future, larger experiments could examine cohesive channel formation in the presence of turbulence, with a constant sediment feed, or with a thin cohesive lid. They could also explore the role of different hydrographs in the presence of cohesion and see how varying boundary conditions such as changing slope and sediment size distribution. While we are confident that increasing %XG increases cohesion, more work needs to be done to quantify cohesive strength and how cohesion alters critical shear stress and transport of sediment in shear flows. Grain scale numerical modelling should complement physical experiments to better understand the mechanics of cohesive sediment transport (Vowinckel et al., 2023).

**ACKNOWLEDGMENTS**

We would like to thank Rory Cottrell, Hesam Askari, and Doug Kelley for their insightful contributions to help improve the quality of the paper.

## REFERENCES CITED

Bennett, S., Casalí, J., Robinson, K., & Kadavy, K. (2000). Characteristics of actively eroding ephemeral gullies in an experimental channel. Transactions of the ASAE, 43. https://doi.org/10.13031/2013.2745.

Bennett, S. J., & Wells, R. R. (2019). Gully erosion processes, disciplinary fragmentation, and technological innovation. *Earth surface processes and landforms*, *44*(1), 46-53.

Brauderick, C. A., Dietrich, W. E., Leverich, G. T., & Sklar, L. S. (2009). Experimental evidence for the conditions necessary to sustain meandering in coarse-bedded rivers. *Proceedings of the National Academy of Sciences*, *106*(40), 16936-16941.

Brunier-Coulin, F., Cuéllar, P., & Philippe, P. (2020). Generalized Shields criterion for weakly cohesive granular materials. *Physical Review Fluids*, *5*(3), 034308.

Chen, C., Wu, L., Perdjon, M., Huang, X., & Peng, Y. (2019). The drying effect on xanthan gum biopolymer treated sandy soil shear strength. *Construction and Building Materials*, *197*, 271-279.

Chen, D., Zheng, J., Zhang, C., Guan, D., Li, Y., & Huang, H. (2022). Threshold of surface erosion of cohesive sediments. *Frontiers in Marine Science*, *9*, 847985.

Church, M., Dudill, A., Venditti, J. G., & Frey, P. (2020). Are results in geomorphology reproducible?. *Journal of Geophysical Research: Earth Surface*, *125*(8), e2020JF005553.

Delenne, J. Y., El Youssoufi, M. S., Cherblanc, F., & Bénet, J. C. (2004). Mechanical behaviour and failure of cohesive granular materials. *International Journal for Numerical and Analytical Methods in Geomechanics*, *28*(15), 1577-1594.

Dunne, K. B., & Jerolmack, D. J. (2018). Evidence of, and a proposed explanation for, bimodal transport states in alluvial rivers. *Earth Surface Dynamics*, *6*(3), 583-594.

Dunne, K. B. J., & Jerolmack, D. J. (2020). What sets river width?. Science Advances, 6, eabc1505. https://doi.org/10.1126/sciadv.abc1505

Julian, J. P., & Torres, R. (2006). Hydraulic erosion of cohesive riverbanks. *Geomorphology*, *76*(1-2), 193-206.

Kothyari, U. C., & Jain, R. K. (2008). Influence of cohesion on the incipient motion condition of sediment mixtures. *Water resources research*, *44*(4).

Malarkey, J., Baas, J. H., Hope, J. A., Aspden, R. J., Parsons, D. R., Peakall, J., ... & Thorne, P. D. (2015). The pervasive role of biological cohesion in bedform development. *Nature communications*, *6*(1), 6257.

Meyer-Peter, E., & Müller, R. (1948). Formulas for bed-load transport.

Moeini, A., Zarandi, N. K., Pazira, E., & Badiollahi, Y. (2015). The relationship between drainage density and soil erosion rate: a study of five watersheds in Ardebil Province, Iran. *WIT Trans Ecol Environ*, *1*, 129-138.

Moragoda, N., Kumar, M., & Cohen, S. (2022). Representing the role of soil moisture on erosion resistance in sediment models: Challenges and opportunities. *Earth-Science Reviews*, *229*, 104032.

G. Parker (1990): Surface-based bedload transport relation for gravel rivers, Journal of Hydraulic Research, 28:4, 417-436

G. Parker, Self-formed straight rivers with equilibrium banks and mobile bed. part 2. The gravel river. J. Fluid Mech. 89, 127–146 (1978)

Perret, J., Prasher, S. O., Kantzas, A., & Langford, C. (1999). Three-dimensional quantification of macropore networks in undisturbed soil cores. *Soil Science Society of America Journal*, *63*(6), 1530-1543.

Peakall, J., Ashworth, P. J., & Best, J. L. (2007). Meander-bend evolution, alluvial architecture, and the role of cohesion in sinuous river channels: a flume study. *Journal of Sedimentary Research*, *77*(3), 197-212.

Phillips, C. and  Douglas J. Jerolmack. Self-organization of river channels as a critical filter on climate signals.*Science***352**,694-697(2016).DOI:10.1126/science.aad3348

Phillips, C.B., Masteller, C.C., Slater, L.J. *et al.* Threshold constraints on the size, shape and stability of alluvial rivers. *Nat Rev Earth Environ* 3, 406–419 (2022).

Rahimnejad, R., & Ooi, P. S. (2016). Factors affecting critical shear stress of scour of cohesive soil beds. *Transportation Research Record*, *2578*(1), 72-80.

Rosalam, S., & England, R. (2006). Review of xanthan gum production from unmodified starches by Xanthomonas comprestris sp. Enzyme and Microbial Technology, 39(2), 197- 207. https://doi.org/10.1016/j.enzmictec.2005.10.019

Sharma, R., Gong, M., Azadi, S., Gans, A., Gondret, P., & Sauret, A. (2022). Erosion of cohesive grains by an impinging turbulent jet. Physical Review Fluids, 7. https://doi.org/10.1103/PhysRevFluids.7.074303

Tal, M., & Paola, C. (2007). Dynamic single-thread channels maintained by the interaction of flow and vegetation. *Geology*, *35*(4), 347-350.

Tal, M., & Paola, C. (2010). Effects of vegetation on channel morphodynamics: results and insights from laboratory experiments. *Earth Surface Processes and Landforms*, *35*(9), 1014-1028.

Thielicke, W., & Sonntag, R. (2021). Particle Image Velocimetry for MATLAB: Accuracy and enhanced algorithms in PIVlab.

Vachtman, D., & Laronne, J. B. (2013). Hydraulic geometry of cohesive channels undergoing base level drop. *Geomorphology*, *197*, 76-84.

Van Dijk, W. M., Teske, R., Van de Lageweg, W. I., & Kleinhans, M. G. (2013). Effects of vegetation distribution on experimental river channel dynamics. *Water Resources Research*, *49*(11), 7558-7574.

Vowinckel, B., Zhao, K., Zhu, R., & Meiburg, E. (2023). Investigating cohesive sediment dynamics in open waters via grain-resolved simulations. *Flow*, *3*, E24.

Zhang, M., & Yu, G. (2017). Critical conditions of incipient motion of cohesive sediments. *Water Resources Research*, *53*(9), 7798-7815.

## FIGURE CAPTIONS

Figure 1: Natural examples of channel patterns and cohesive banks. A)  Braided Toklat River in Alaska, USA. B) Single thread meandering Genesee River in Rochester, NY, USA; C:

Retreating head-cut in Utah, USA; D: Cohesive channel banks in Little Piney Run, a small tributary in Baltimore, MD, USA; E: Cohesive banks of Minebank Run in Towson, Baltimore, MD, USA.

Figure 2: A) Experimental flume setup in the laboratory using Global King Inc W15GR-15A pump. B) Illustration of the steps involved in Particle Image Velocimetry (PIV) used to generate the particle velocities of each grain, facilitating the continuous visualization of the active channel for 0.1% xanthan gum, and imageJ illustration of hand-drawn extraction of bank widths. C) Microscope image showing xanthan gum bonds between sediment grains when wet and dry. Dry XG bonds strongly resemble water capillary bridges.

Figure 3: Representative images from each experiment with different %XG. 0-0.1%XG were captured in at minute 10 of the experiments. 0.2-0.3%XG images were captured at minute 40. 0.4-0.5% were captured at minute 50.

Figure 4: Data show A) Spatially averaged channel bank widths over time with standard deviation. B) headcut location over time for different %XG, each fitted with Eqn. 1. (C) PIV-derived active channel velocities with standard deviation on the left axis. Time and space averaged channel widths with standard error of the mean on the bars are shown on right axis.

## SUPPLEMENTARY MATERIALS

### SI1: Detailed Methods

**Persistence of cohesion when submerged**: Before the first initialization of the experiments described below, we conducted a series of preliminary experiments mixing xanthan gum with plastic particles and cutting them into cubic aggregates to see how well xanthan gum binds with the particles underwater and observe if there will be any dissolution for over a long period of time. We saw that the aggregates remained cohesive when held under water for at least 10 minutes, demonstrating that cohesive strength remains even when submerged. While it was not possible to measure in our experiments, it is likely that after longer periods of submersion there is a decrease in the strength of the xanthan gum bonds.

**Reynolds Number:** To estimate the Reynolds Number in our setup, we did an estimation by using the depth of the notch (2cm), velocities from the flow rates (25L/h, 40L/h, 55L/h) knowing discharge $Q = A * U$ where A is notch area ($2cm^2$) U is velocity, density of water (1000kg/$m^3$), and dynamic viscosity of water 1 mPa.s. While some turbulence likely occurred in our experiments, we estimate that the Reynolds number of the experiments ranged from ~600-1500, well within the laminar-transitional range. We also conducted a flow visualization water test by introducing green dye into the water, and we observed that the dye maintained a smooth parallel path indicating a predominantly laminar flow. Before reaching the inlet, water from the pump passed through a layer of Styrofoam to regulate the flow and decrease turbulence. A layer of small gravel was placed at the outlet wall to stabilize the flume outlet section to manage flow patterns and minimize undesirable turbulence or scour at the wall.

**Image analysis and PIV:** To measure sediment transport velocities, we employed PIVlab, a particle image velocimetry tool which is instrumental in tracking the velocities of particles across pairs of images (Thielicke, 2021). MATLAB was utilized to process video recordings by converting them into discrete image frames. To enable efficient processing, we analyzed a subset of images for each video. For the initial range of 0% to 0.3%XG, video analysis commenced every 10th image. In contrast, for concentrations of 0.4% and 0.5%, image extraction was performed every 50th frame. This methodology was necessitated by the slower particle movement induced by increased cohesion, which required a more significant interval to capture meaningful changes in pixel pairs. After the initial image extraction, we employed PIVlab for comprehensive image preprocessing. Selected image pairs were analyzed every 300 frames within each session, during which we conducted filtering and enhancement operations on the images. A region of interest (ROI) was defined and consistently applied throughout each video analysis, with distinct ROIs utilized for different experimental conditions. Careful selection of the ROIs was executed to exclude the influence of the flume walls from the analysis. The Particle Image Velocimetry (PIV) algorithm implemented was multipass Fast Fourier Transform (FFT) window deformation, comprising four passes: the first pass utilized an integration area of 128 with a step size of 32 units, while the fourth pass employed an interrogation area of 8. Velocity limits were set to range from -1 to 1 in both the x and y directions, and the mean velocities were subsequently calculated and exported. Following this process, we imported the various processing sessions for each video into the MATLAB interface, allowing us to extract the x and y velocities from the original data provided by the PIV analysis. From these velocity components, we computed the magnitude of the velocities and subsequently generated a binarized image using a threshold range 0.3 to 0.5. To improve clarity, we applied image filtering and enhancement techniques such as morphological operations to close gaps between white pixels and reduce blurriness, and a function to extract the largest channel and remove the unwanted small blobs (see Appendix B). We then selected the middle white channel for analysis and removed isolated white blobs outside of the main channel to refine the binary image for further analysis. (Figure 2C).

To complement the PIV analysis and measure total bank width and headcut retreat rates, we used simple image analysis in ImageJ. We drew a series of lines across the channel for each minute of the first 10 minutes of each video (when channel adjustment is most active), then for approximately every 10 minutes thereafter depending on whether changes in width were observed in the videos. Reflection of light on the water surface clearly delineates the location of headcuts (in experiments where headcuts occur). Attempts to automate identification of the channel banks from images were not successful due to the lack of high contrast in our images.

**2.5 Calculation of Steady State**

To understand how head cuts retreat, and banks widen over time, we used a simple model to describe each dataset with an exponential formula:

$w(t), h(t) = wf, hf(1-e-t/ts)$.

In this formula, $w(t)$ and $h(t)$ represent the width and head cut position or channel at time t, while wf and hf are the final steady-state values. The term ts indicates the timescale for adjustment. This model shows how each dataset moves toward equilibrium in different concentrations of xanthan gum.

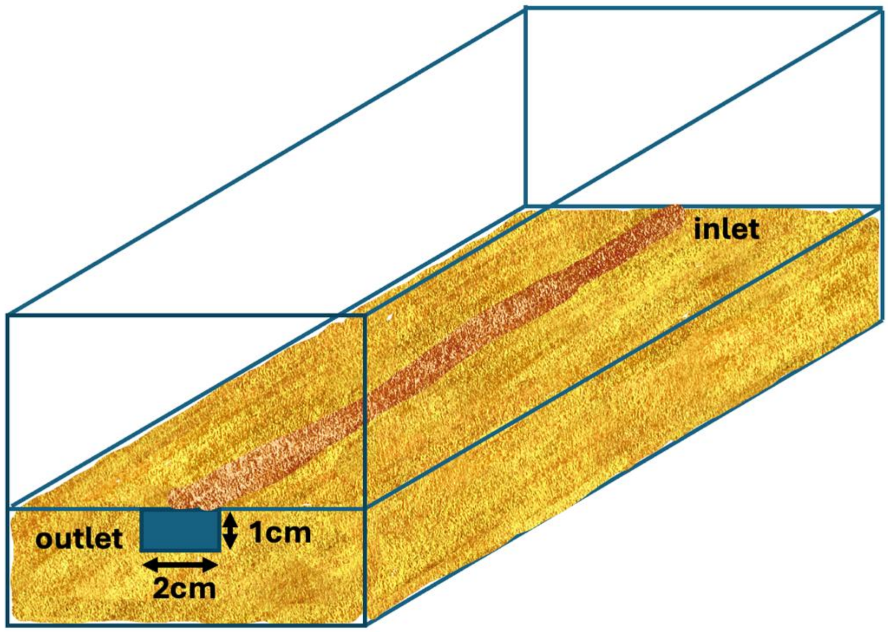


Figure S1: cartoon of flume setup with notch cut at outlet. Darker brown indicates gently scraped channel at beginning of experiment

**SI2: Replicated Experiments**

Images from a second set of experiments (Appendix B) generally show similar behavior to the experiments analyzed here, with increasing cohesion leading to single thread channels with retreating headcuts. However, the channel remains straight for 0.1%XG, likely due to slightly different morphology of the initial scraped channel. We also observe small side channels forming for the 0.2%XG run. These differences highlight the nonlinearity of channel formation processes, where even slightly initial conditions can result in different behavior. Further, it is likely that even mixtures with the same %XG were not identical due to slight variations in xanthan gum content and distribution throughout the material. While many more experiments would be needed to obtain a reproducible statistical distribution of channel forms, though this remains a grand challenge in geomorphology, where experiments are time consuming to run, and reproducibility between different experiments is notoriously difficult to obtain (Church et al., 2020). Aside from these considerations, it is encouraging that the second set of experiments generally show the same behavior as the first—increasing cohesion fundamentally and qualitatively alters channel morphology.

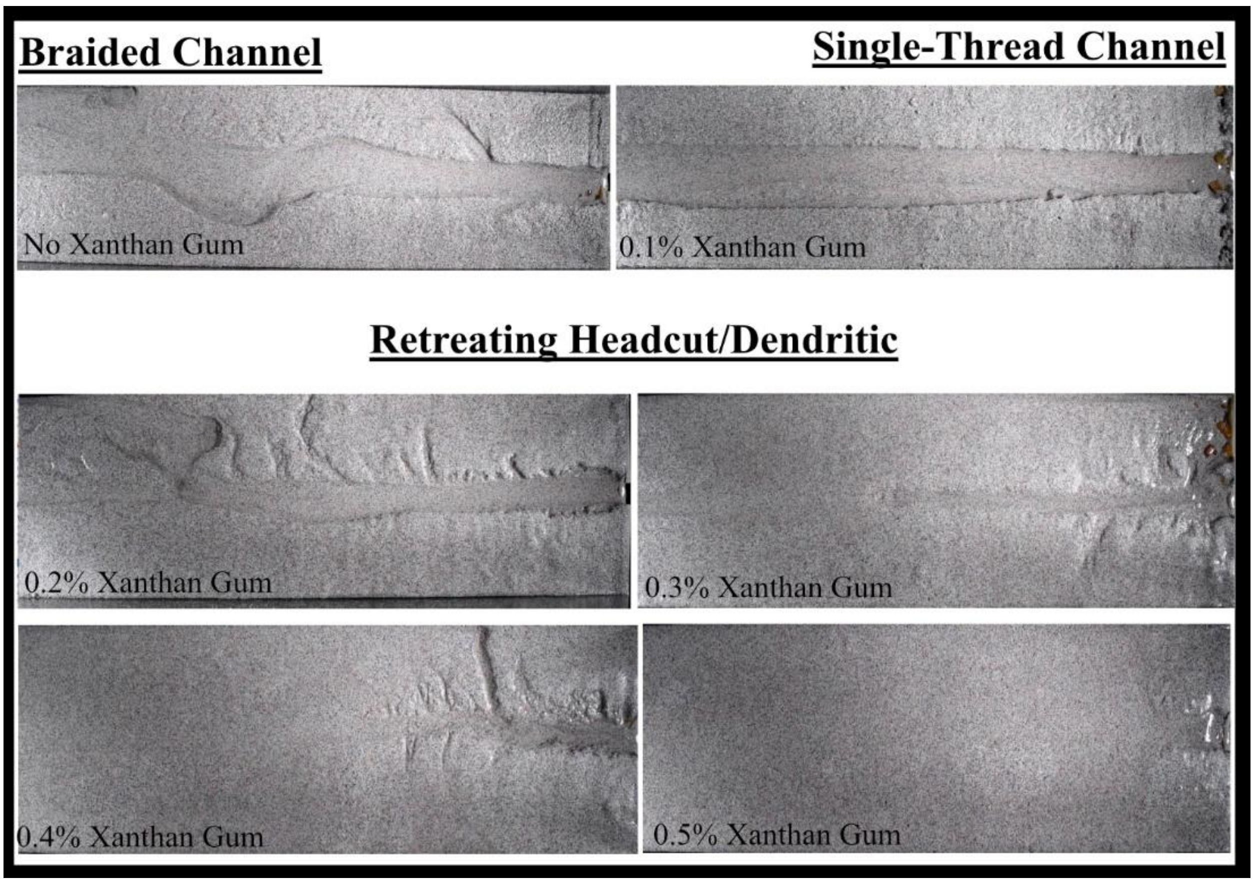


Figure S2: Representative images of a second set of experiments from each experiment with different %XG. 0-0.1%XG were captured in at minute 40 and 30 of the experiments, respectively. 0.2-0.3%XG images were captured at minute 40. 0.4-0.5% were captured at minute 50 and 40 respectively.

[1]Supplemental Material. This material summarizes the MATLAB codes developed for image processing, data extraction, and flow analysis throughout the experiments.

Please visit https://github.com/nacere14/-EXPERIMENTS-ON-THE-ROLE-OF-COHESION-IN-RIVER-MORPHODYNAMICS/tree/main to access the supplemental material, and nsamassi@ur.rochester.edu with any questions.